NASA TECHNICAL MEMORANDUM

NASA TM X-2235

NASA TM X-2235

DESIGN AND PERFORMANCE OF A 0.9-HUB-TIP-RATIO AXIAL-FLOW PUMP ROTOR WITH A BLADE-TIP DIFFUSION FACTOR OF 0.63

by Donald C. Urasek

Lewis Research Center
Cleveland, Ohio 44135

NATIONAL AERONAUTICS AND SPACE ADMINISTRATION • WASHINGTON, D. C. • MARCH 1971

1. Report No. NASA TM X-2235	2. Government Accession No.	3. Recipient's Catalog No.
4. Title and Subtitle DESIGN AND PERFORMANCE OF A 0.9-HUB-TIP-RATIO AXIAL-FLOW PUMP ROTOR WITH A BLADE-TIP DIFFUSION FACTOR OF 0.63		5. Report Date March 1971 6. Performing Organization Code
7. Author(s) Donald C. Urasek		8. Performing Organization Report No. E-5765
9. Performing Organization Name and Address Lewis Research Center National Aeronautics and Space Administration Cleveland, Ohio 44135		10. Work Unit No. 128-31 11. Contract or Grant No.
12. Sponsoring Agency Name and Address National Aeronautics and Space Administration Washington, D.C. 20546		13. Type of Report and Period Covered Technical Memorandum 14. Sponsoring Agency Code

15. Supplementary Notes

16. Abstract

A 9-inch- (22.9-cm-) diameter axial-flow rotor with a 0.9 hub-tip radius ratio, a design flow coefficient of 0.70, and a blade-tip diffusion factor of 0.63 was tested in cold water under both cavitating and noncavitating conditions. Radial surveys of the flow conditions at the blade inlet and outlet were made. At design flow, the rotor produced an overall head-rise coefficient of 0.537 with an overall efficiency of 92.0 percent. The efficiency remained high over the entire flow range.

17. Key Words (Suggested by Author(s))

Axial-flow pump rotor
0.9 hub-tip ratio
Tip D-factor, 0.63
Design flow coefficient, 0.70

18. Distribution Statement

Unclassified - unlimited

19. Security Classif. (of this report)	20. Security Classif. (of this page)	21. No. of Pages	22. Price*
Unclassified	Unclassified	33	$3.00

*For sale by the National Technical Information Service, Springfield, Virginia 22151

DESIGN AND PERFORMANCE OF A 0.9-HUB-TIP-RATIO AXIAL-FLOW PUMP ROTOR WITH A BLADE-TIP DIFFUSION FACTOR OF 0.63

by Donald C. Urasek

Lewis Research Center

SUMMARY

A 9-inch- (22.9-cm-) diameter axial-flow rotor with a 0.9 hub-tip radius ratio, a design flow coefficient of 0.70, and a blade-tip design diffusion factor of 0.63 was tested. The tests were conducted in 80° F (26.7° C) water under both cavitating and noncavitating flow conditions. Detailed radial surveys of the flow conditions at the blade inlet and ouetlet were made, and flow and performance parameters were calculated across a number of selected blade elements. The stall hysteresis was recorded at three blade element locations, and definitions of the outer casing boundary layer were made at the blade inlet and outlet measuring stations.

At design flow, the rotor produced an overall head-rise coefficient of 0.537 as compared to the design value of 0.558. An overall efficiency of 92.0 percent was achieved experimentally as compared to a design value of 86.5 percent. The efficiency remained high over the entire flow range.

The rotor would not recover from a stalled operating condition by opening the throttle valve while operating at constant rotative speed and inlet pressure. Stall recovery was achieved by lowering the inlet pressure.

INTRODUCTION

Axial-flow pumps offer the advantages of simple staging and blade design control through the use of a blade element design system. One objective of an axial pump design is to limit the number of stages comprising a pump configuration. Using a minimum number of stages to produce the required pressure rise results in a smaller pump with reduced mechanical complexity. Thus, each individual stage should be designed to produce the maximum possible head-rise within limits imposed by high blade loading. Herein, a measure of blade loading is provided by the diffusion factor (D-factor) devel-

oped in reference 1. The level of blade loading must be consistent with acceptable values of efficiency and stable operating flow range.

The experimental investigations reported in references 2 and 3 showed that a 9-inch- (22.9-cm-) diameter 0.8 hub-tip-ratio axial-flow rotor having a D-factor of 0.66 and a flow coefficient of 0.452 performed satisfactorily. At design flow, the rotor produced an overall head-rise coefficient of 0.391 as compared to the design value of 0.427. An overall efficiency of 95.5 percent was achieved experimentally which compares with the design value of 92.8 percent.

A velocity diagram study, which assumed no inlet whirl and no change in axial velocity across the rotor, showed that for a given level of blade loading (D-factor) the ideal head-rise coefficient was increased as the inlet flow coefficient was increased (ref. 2). When low inlet pressure is required, it is necessary to match a high flow coefficient stage with an inducer that would provide good cavitation performance. The inducer usually requires a low flow coefficient. Thus, a highly loaded stage with a high flow coefficient would require a considerable annulus area contraction ahead of the rotor. Such a highly loaded stage would be designed with a high hub-tip ratio. The rotor blades are quite short so that three-dimensional flows in blade end regions have significant effects on the performance of this type of stage.

In the investigation reported herein, the performance of a highly loaded pump rotor operating with a design flow coefficient of 0.70 is evaluated. The 9-inch- (22.9-cm-) diameter axial-flow pump rotor had a hub-tip ratio of 0.9 and a tip D-factor of 0.63. The rotor tests were conducted in 80° F (26.7° C) water at a rotative speed of 2500 rpm. This report presents the blade design, the measured overall performance, and the blade element performance for noncavitating flow conditions. In addition, variations of flow conditions and performance of a selected number of blade elements over a range of operating modes are shown. As flow was reduced into the blade stall region, the stall hystereses were measured and are shown at three radial blade element locations. Limited data taken at reduced inlet pressure are presented to indicate the level of inlet pressure required for this stage to operate with no loss in performance. Finally, measurements were made to define the outer wall boundary layer at the blade inlet and outlet measuring stations.

ROTOR DESIGN

The design for this rotor used a blade element flow theory. The velocity diagram calculations and the blade section profile designs were conducted across a number of surfaces of revolution which were cylindrical. The blade elements were stacked on a radial line through the center of gravity of the individual sections.

The selected design values for this rotor are

(1) Flow coefficient, $\varphi = 0.70$

(2) D-factor at tip, 0.63

(3) Hub-tip ratio, 0.90

(4) Tip diameter, 9 inches (22.9 cm)

As explained in the INTRODUCTION and in reference 2, for a highly loaded blade, a high hub-tip ratio would probably be associated with the high flow coefficient. The blade element design procedure used is similar to that described in detail in reference 2 with the following exceptions. Because of the high hub-tip ratio and diameter of this rotor, three-dimensional flows were expected to affect the losses over a large portion of the blade passage. Since this type of loss could not be accounted for directly in the design procedure, values of total head-loss coefficient $\overline{\omega}$ and ideal head-rise coefficient ψ_{id} were chosen to be radially constant over the blade height. The velocity diagram design values computed for this rotor are shown in table I. The values are based on no inlet prewhirl. The blade design values are listed in table II. A photograph of the rotor is shown in figure 1.

APPARATUS AND PROCEDURE

Test Facility

The rotor was tested in the Lewis water tunnel which is described in detail in reference 4. A schematic diagram of the test facility is shown in figure 2. Before the tests, the water in the loop was conditioned by reducing the gas content to approximately 1 ppm by weight and by circulating the water through a filter capable of removing solid particles larger than 5 microns. During tests, the gas content was maintained below 3 ppm by weight, and the water temperature was maintained at approximately 80° F (26.7° C).

Test Procedure and Instrumentation

The noncavitating performance characteristics were obtained by maintaining the inlet pressure and rotative speed constant while varying flow. At each selected flow, the radial distributions of flow conditions were surveyed at measuring stations located approximately 1 inch (2.54 cm) upstream of the blade leading edge and 0.6 inch (1.52 cm) downstream of the blade trailing edge. Measurements of total pressure, static pressure, and flow angle were recorded at radial positions of 10, 30, 50, 70, and 90 percent of the passage height from the outer walls (designated RP-10, 30, 50, 70, and 90, respectively). Blade elements were assumed to lie on cylindrical surfaces intersecting these radial positions.

Two methods to obtain cavitation performance were (1) holding blade speed and flow constant while reducing the inlet pressure from a high noncavitating value and (2) holding blade speed and inlet pressure constant while varying the flow. Measurements of total pressure, static pressure, and flow angle were recorded at 50 percent of passage height (RP-50) for these tests.

Photographs of the survey probes are shown in figure 3. Total pressure and flow angle were measured with the cobra probe (fig. 3(a)), and static pressure was measured with the wedge probe (fig. 3(b)). Each probe had associated null-balancing, stream-direction, sensitive equipment that automatically alined the probe to the direction of flow. Each wedge static probe was calibrated in a low speed air tunnel. Additional instruments included a venturi flowmeter to measure flow rate and an electronic speed counter used in conjunction with a magnetic pickup to measure rotor rpm.

The distribution of total pressure and flow angle across the boundary layer on the outer wall was measured with the probe shown in figure 3(c). Boundary layer surveys were taken at three flow coefficient values under noncavitating flow conditions.

Data Accuracy and Reliability

The estimated minimum errors of the data based on inherent accuracies of the instrumentation and recording systems are as follows:

Flow rate, Q_V, percent of rotor design flow	±1.0
Rotative speed, N, percent	±0.5
Blade element head rise, ΔH, percent at design flow	±1.0
Velocity head, $V^2/2g$, percent at design flow	±1.5
Flow angle, β, deg	±1.0
Net positive suction head, NPSH, ft (m)	±1.0(0.3)

The influence of secondary flows, unsteady flows, circumferential variations of flow, etc. on the accuracies of the data were not evaluated. The symbols are defined in appendix A. The equations used for calculating the selected blade element and overall performance parameters are presented in appendix B.

The primary method for determining the reliability of the measured data is through comparisons of the integrated weight flows at the blade inlet and the outlet measuring stations with the values measured with the venturi meter. These comparisons are presented in figure 4. At flow coefficients greater than 0.69, the integrated flows at the outlet are within 4 percent of the venturi flow. At flow coefficient less than 0.69, the integrated flows deviate significantly from the venturi as the rotor approaches a stall condition. The integrated flows at the inlet measuring station were within 3.5 percent

of the venturi flow. The flow checks generally indicate a reasonable agreement of measured data.

RESULTS AND DISCUSSION

Overall Performance

Noncavitating. - The noncavitating overall performance curves are shown in figure 5 where mass averaged rotor head-rise coefficient $\overline{\psi}$ and mass averaged efficiency $\overline{\eta}$ are plotted as functions of average flow coefficient $\overline{\varphi}$. The average flow coefficient is based on venturi measured flow, inlet geometric area, and blade-tip speed as defined in appendix B. The characteristic curve was limited at low flows by unstable flow conditions evidenced by rig vibrations and noise (stalled condition) and at high flows by the pressure loss characteristic of the test loop.

From the casing boundary layer measurements (see appendix C), a flow blockage factor of 4.35 percent was determined for design flow at the rotor inlet. (A flow blockage factor of 2.76 percent was computed at the rotor outlet.) Thus, the design inlet flow diagrams should be achieved at a measured average flow coefficient of

$$\overline{\varphi} = (1.0 - 0.0435)\overline{\varphi}_{des}$$

$$\overline{\varphi} = 0.9565\ (0.70) = 0.670$$

The flow coefficient of 0.670 is used hereinafter as the design value in comparison of measured and design parameters. At $\overline{\varphi} = 0.670$, the measured head-rise coefficient of 0.536 is slightly below the design value of 0.558. Design efficiency was 86.5 percent, while an overall efficiency of 92.0 percent was achieved experimentally. The data show that the efficiency remained high (greater than 88 percent) over the entire flow range.

Cavitating. - A limited amount of cavitation data was obtained for this highly loaded rotor to determine the net positive suction head (NPSH) at which performance of such a main stage rotor is affected by cavitation. The rotor head-rise coefficient ψ, which was measured at the midpassage station (RP-50), is plotted in figure 6 as a function of NPSH at an average flow coefficient $\overline{\varphi}$ of 0.70. At this flow coefficient the performance started to deteriorate because of cavitation at a NPSH value of 280 feet (85.5 m) and a blade-tip speed of 99 feet per second (30 m/sec).

Additional cavitating characteristic performance curves are presented in figure 7 where rotor head-rise coefficient ψ measured at midpassage (RP-50) is plotted over the range of flows for four values of NPSH. A noncavitating NPSH value of 435 feet (133 m) is plotted to provide a basis for comparison.

BLADE ELEMENT PERFORMANCE

Radial Distributions

The noncavitating radial distribution of selected flow and performance parameters at five flow coefficients is shown in figure 8. The design values are shown by the dotted lines. The discussion in this section is directed to general performance trends indicated by the data and is applicable to all operating points.

The inlet total head (fig. 8(a)) drops off significantly in both the hub and tip regions of the rotor blade. As shown by the boundary layer measurements in appendix C, the casing boundary layer thickness extends to approximately 20 percent of span at the rotor tip. Boundary layer results are further discussed in appendix C. If the same boundary layer is assumed at the hub, the 90-percent station (RP-90) is being affected in a similar manner as at RP-10. Lower flow at RP-10 and RP-90 should increase the incidence angle at these locations as verified by figure 8(b). The boundary layer losses also show up in the inlet flow coefficient distribution (fig. 8(d)). It appears that the higher losses in the hub and tip regions caused the higher flow coefficients near the mean blade height.

The radial distributions of parameters describing flow at the rotor outlet indicate strong three-dimensional effects. For example, the loss coefficient distribution (fig. 8(e)) shows a sharp increase in losses in both the hub and tip regions. These high losses in the tip region have been observed on other rotors (ref. 5). However, in contrast to the rotors discussed in reference 5, a high loss has also been observed in the hub region of this 0.9 hub-tip ratio rotor. A high loss region extends over a greater radial portion of the blade from the hub region than in the tip region for this blade. This may have aided in reducing the measured losses in the tip region. Even with the small blade height of 0.45 inch (1.14 cm) the blade did have a low loss flow region in the central part of the blade.

The other parameter reflecting three-dimensional flow effects was the deviation angle shown in figure 8(k). Consideration of two-dimensional flow only would result in radial distribution of deviation angle shown by the design distribution in the figure. The measured distribution, which includes three-dimensional flow effects, shows significant differences in both level and distribution. In reference 5, a 0.7 hub-tip radius ratio rotor having a design flow coefficient value of 0.284 showed a radial distribution approximating the design distribution, based primarily on two-dimensional flow considerations. However, a 0.8 hub-tip radius ratio rotor having a design flow coefficient of 0.451 showed a radial distribution of deviation angle similar to that shown in figure 8(k). The predicted deviation angles, which are based on two-dimensional flow, appear to be grossly inadequate for rotors affected by three-dimensional flows.

The deviation angle and the incidence angle reflect the amount of fluid turning according to

$$\Delta\beta' = \varphi^{O} + i - \delta$$

The radial distribution of other parameters reflect the effects of distributions of fluid turning, outlet flow coefficient, and flow losses.

Variations with Incidence Angle

The variations of selected blade element performance parameters with incidence angle are presented in figure 9 for five blade elements designated as RP-10, 30, 50, 70, and 90.

The incidence angle at which minimum loss occurred could only be designated at the RP-10 radial station. The minimum loss incidence angle was approximately -8^{O}, which was about equal to the design value at this station. The maximum efficiency point for this radial station is coincident with the minimum loss operating point (-8^{O}).

The loss coefficient $\overline{\omega}$ is increasing at the RP-10 station as the rotor approaches stall (increasing incidence angle), while at RP-50, 70, and 90 stations, there is no tendency for $\overline{\omega}$ to increase as the rotor approaches a stall condition. The RP-30 station is not clearly defined but does appear to be increasing only very slightly as the rotor approaches stall. This trend in loss coefficient indicates that the tip portion of the rotor blade may have stalled first at an incidence angle of approximately 3.4^{O}. At the point of stall, the D-factor at the RP-10 station was very high, 0.71.

At radial measuring stations RP-50, 70, and 90, the deviation angle showed the tendency to increase as the rotor approached both maximum flow and stall.

Stall Performance

The complete noncavitating performance curve of the rotor, including the stall region, is shown in figure 10 where the rotor head-rise coefficient for three blade elements is plotted as a function of average flow coefficient. The open symbols are data recorded on an automatic voltage digitizer and computed using a digital computer, while the solid symbols were data recorded on an X-Y plotter. The use of the X-Y plotter greatly reduces the amount of time spent in the stall region and consequently reduces the chance of possible pump damage in this mode of operation. As flow was reduced from the maximum value, the head-rise coefficient increased to a peak value and then decreased to point A at a flow coefficient of 0.52. Any further throttling beyond point A forced the pump into a stalled condition at a flow coefficient value of 0.25 (point B). Pump operation between points A and B was not possible. When the throttle valve was opened the pump operating point moved from point B to point C. Data were not recorded

between these two points; operation in this condition was limited because of possible damage to the pump.

With the throttle valve wide open, the pump would not come back out of stall. The pump remained at the operating condition of point C. At a constant rotative speed, the only way to bring the pump out of a stalled condition was to reduce the NPSH to a value of approximately 100 feet (30.5 m) and thereby cause the pump to cavitate. This maneuver shifted the operating point from point C to point D. Therefore, point D is a stable operating point; however, the pump is highly cavitated at this point. To return the pump to its noncavitating flow condition (point E), the NPSH was increased to its noncavitating value.

SUMMARY OF RESULTS

A 9-inch- (22.9-cm-) diameter axial flow rotor with a 0.9 hub-tip radius ratio, a design flow coefficient of 0.70, and a blade-tip design diffusion factor of 0.63 was tested. The tests were conducted in 80° F (26.7° C) water under both cavitating and noncavitating flow conditions. Detailed radial surveys of the flow conditions at the blade inlet and outlet were made, and flow and performance parameters were calculated across a number of selected blade elements. The stall hysteresis was recorded at three blade element locations and definitions of the outer casing boundary layer were made at the blade inlet and outlet measuring stations. From the tests, the following principal results were obtained:

1. At the design flow coefficient, the rotor produced an overall head-rise coefficient of 0.536 as compared to the design value of 0.558. An overall efficiency of 92.0 percent was achieved experimentally which compares with the design value of 86.5 percent

2. The efficiency remained high (>88 percent) over the entire flow coefficient range which varied from 0.585 to 0.820.

3. The inlet boundary layers at both the hub and tip of the rotor caused the flow to be redistributed at the rotor inlet. This resulted in an inlet velocity gradient across the blade passage. From the outer wall boundary layer measurements, flow blockage values of 4.35 percent at the blade inlet and 2.76 percent at the blade outlet were computed.

4. The radial distributions of parameters describing flow at the rotor outlet indicate that strong three-dimensional flows have affected the loss and deviation angle distributions.

5. The blade-tip diffusion factor was 0.71 at a stalled operating condition of the rotor.

6. The rotor would not recover from a stalled operating condition by opening the throttle valve at constant rotative speed and inlet pressure. Stall recovery was achieved by lowering the inlet pressure while operating at a constant rotative speed.

7. At the design flow coefficient and rotor-tip speed of 99 feet per second (30 m/sec) the rotor performance started to deteriorate due to cavitation at a net positive suction head value of 280 feet (85.5 m).

Lewis Research Center,
National Aeronautics and Space Administration,
Cleveland, Ohio, November 24, 1970,
128-31.

APPENDIX A

SYMBOLS

A	annulus area, ft (m)
C	blade chord, in. (cm)
D	blade diffusion factor, eq. (B8)
g_c	standard acceleration of gravity, 32.174 $(lb_m)(ft)/(lb_f)(sec^2)$ (9.8 M/sec^2)
H	total head, ft (m)
h_v	vapor pressure head, ft (m)
ΔH	blade element head rise, ft (m)
$\overline{\Delta H}$	mass averaged head rise, ft (m)
i	incidence angle, eq. (B9), deg
NPSH	net positive suction head, ft (m), eq. (B17)
Q_v	venturi measured flow rate, gal/min (m^3/min)
RP	radial position
r	radius, ft (m)
T	thickness, ft (m)
V	velocity, ft/sec (m/sec)
β	flow angle, deg
$\Delta\beta'$	turning angle, deg
δ	deviation angle (used as a limit of integration in eqs. (B18) and (B19))
δ^*	displacement thickness, eq. (B18)
η	hydraulic efficiency, eq. (B5)
$\overline{\eta}$	mass averaged hydraulic efficiency, eq. (B14)
θ	momentum thickness, eq. (B19)
κ	blade angle, deg
σ	blade solidity
φ	flow coefficient, eq. (B6)
φ^o	blade camber angle, deg
$\overline{\varphi}$	average flow coefficient, eq. (B16)
ψ	head-rise coefficient, eq. (B2)
$\overline{\psi}$	mass averaged head-rise coefficient, eq. (B12)
$\overline{\omega}$	rotor relative total head-loss coefficient, eq. (B7)

Subscripts:

b	blocked
des	design
f.s.	free stream
h	hub
IW	inner wall
id	ideal
j	index number
MAX	maximum
OW	outer wall
T	total
t	tip
v	measured with venturi flowmeter
z	axial component
θ	tangential component

1 rotor inlet

2 rotor outlet

Superscript:

' relative to rotor

APPENDIX B

EQUATIONS

The equations used to calculate the blade element and overall performance parameters are now given.

Blade Element Equations

Blade element head rise:

$$\Delta H = H_2 - H_1 \tag{B1}$$

Rotor head-rise coefficient:

$$\psi = \frac{g\,\Delta H}{U_t^2} \tag{B2}$$

Ideal head rise:

$$\Delta H_{id} = \frac{U_2 V_{\theta,2} - U_1 V_{\theta,1}}{g} \tag{B3}$$

Ideal head-rise coefficient:

$$\psi_{id} = \frac{g\,\Delta H_{id}}{U_t^2} \tag{B4}$$

Hydraulic efficiency:

$$\eta = \frac{\Delta H}{\Delta H_{id}}\,100 \tag{B5}$$

Flow coefficient:

$$\varphi = \frac{V_z}{U_t} \tag{B6}$$

Rotor relative total head-loss coefficient:

$$\overline{\omega} = \frac{H'_{2,id} - H'_2}{\frac{V'^2_1}{2g}} = \frac{\Delta H_{id} - \Delta H}{\frac{V'^2_1}{2g}} \tag{B7}$$

Blade diffusion factor:

$$D = 1 - \frac{V'_2}{V'_1} + \frac{r_2 V_{\theta,2} - r_1 V_{\theta,1}}{\sigma V'_1 (r_1 + r_2)} \tag{B8}$$

or, for $r_1 = r_2$,

$$D = 1 - \frac{V'_2}{V'_1} + \frac{\Delta V_\theta}{2\sigma V'_1}$$

Incidence angle:

$$i = \beta'_1 - \kappa_1 \tag{B9}$$

Turning angle:

$$\Delta\beta' = \beta'_1 - \beta'_2 \tag{B10}$$

Overall and Averaged Parameter Equations

Mass averaged head rise:

$$\overline{\Delta H} = \frac{\sum_{j=1}^{j=4} (r_j V_{z,2,j} \Delta H_j + r_{j+1} V_{z,2,j+1} \Delta H_{j+1})(r_j - r_{j+1})}{\sum_{j=1}^{j=4} (r_j V_{z,2,j} + r_{j+1} V_{z,2,j+1})(r_j - r_{j+1})} \tag{B11}$$

Mass averaged head-rise coefficient:

$$\overline{\psi} = \frac{g\,\overline{\Delta H}}{U_t^2} \tag{B12}$$

Mass averaged ideal head rise:

$$\overline{\Delta H}_{id} = \frac{1}{g}\overline{U_2 V_{\theta,2}} - \overline{U_1 V_{\theta,1}} = \frac{1}{g}\left(\frac{\sum_{j=1}^{j=4} U_{2,j} V_{\theta,2,j} A_{2,j} V_{z,2,j}}{\sum_{j=1}^{j=4} A_{2,j} V_{z,2,j}}\right) - \left(\frac{\sum_{j=1}^{j=4} U_{1,j} V_{\theta,1,j} A_{1,j} V_{z,1,j}}{\sum_{j=1}^{j=4} A_{1,j} V_{z,1,j}}\right) \tag{B13(a)}$$

In this investigation $V_{\theta,1}$ was considered zero in all calculations, and so the equation becomes

$$\overline{\Delta H}_{id} = \frac{1}{g}\left(\frac{\sum_{j=1}^{j=4} U_{2,j} V_{\theta,2,j} A_{2,j} V_{z,2,j}}{\sum_{j=1}^{j=4} A_{2,j} V_{z,2,j}}\right) = \frac{\overline{U_2 V_{\theta,2}}}{g} \tag{B13(b)}$$

Mass averaged efficiency:

$$\overline{\eta} = \frac{\overline{\Delta H}}{\overline{\Delta H}_{id}} 100 \tag{B14}$$

Average inlet axial velocity:

$$\overline{V}_{z,1} = \frac{Q_v}{k\pi\left(r_{t,1}^2 - r_{h,1}^2\right)} \tag{B15}$$

where $k = 448.8$ feet per second (60 m/sec).

Average inlet flow coefficient:

$$\overline{\varphi} = \frac{\overline{V}_{z,1}}{U_t} \tag{B16}$$

Net positive suction head:

$$NPSH = \overline{H}_1 - h_v \tag{B17}$$

Boundary layer parameter equations:

$$\delta^* = \int_0^{\delta} \left(1 - \frac{V_z}{V_{z,f.s.}}\right) dy \tag{B18}$$

and

$$\theta = \int_0^{\delta} \frac{V_z}{V_{z,f.s.}} \left(1 - \frac{V_z}{V_{z,f.s.}}\right) dy \tag{B19}$$

where δ is the limit of integration in inches (cm).

APPENDIX C

OUTER WALL BOUNDARY LAYER MEASUREMENTS

Surveys of flow conditions across the outer wall boundary layer were made at the blade inlet and outlet measuring stations for a range of flows. The measurements were used primarily to obtain flow blockage values.

The velocity profiles at the blade inlet measuring station are shown in figure 11. The velocities are computed from boundary layer surveys of total pressure and angle, and wall static pressure measurements. The boundary layer parameters, displacement thickness δ^*, and momentum thickness θ were computed from the velocity profiles shown.

At the inlet measuring station, angle measurements indicated that the flow direction was essentially axial, and thus, the boundary layer was considered two-dimensional. Boundary layer measurements were made out to the RP-30 station (0.135 in. (0.343 cm) from the outer wall). The velocity distribution showed that a constant free-stream velocity was maintained to approximately 0.080 inch (0.204 cm) from the outer wall. The velocities are presented as the ratio of local velocity to free-stream velocity where free-stream velocity is defined as the value measured at the RP-30 radial location (see fig. 11). The velocity ratio distribution was essentially the same over the whole flow range of the rotor. The boundary layer thickness was set at 0.080 inch (0.204 cm) in all flow parameter calculations at the inlet. The computed values of δ^* and θ were 0.0098 and 0.0085 inch (0.0249 and 0.0216 cm), respectively. The value of displacement thickness for the hub shroud was computed in a similar manner. Area blockage factors were computed for both inner and outer walls and are presented in table III as the ratio of the blocked area (A_b) to the total annulus area (A) in percent. With a flow blockage of 4.35 percent, the design inlet flow diagrams should be achieved at a measured average flow coefficient:

$$\overline{\varphi} = (1 - 0.0435)\overline{\varphi}_{des}$$

$$\overline{\varphi} = (0.9565)(0.70) = 0.670$$

At the blade outlet measuring station, the boundary layer flow has both axial and tangential velocity components. This skewed boundary layer flow is further complicated by the 0.010-inch (0.025-cm) tip clearance between the housing and the rotating blade. For these reasons, calculation of boundary layer parameters at this axial station was limited to a displacement thickness based on the through flow velocity component V_z. The axial and tangential components of the boundary layer velocities are presented in figures 12 and 13, respectively. As shown by the survey of outlet axial velocity, the

free-stream value was maintained to a radial location of approximately 0.045 inch (0.114 cm) from the outer wall. Thus, the boundary layer thickness was set at 0.045 inch (0.114 cm) in the displacement thickness calculations.

The velocity distribution was essentially the same over the flow range of the rotor, and a single faired curve was used to compute a value of δ^* equal to 0.0062. Area blockage was computed for both the inner and outer walls at the outlet measuring station using this same value of δ^* for the hub shroud. The results are shown in table III.

Two observations were made. First, the blockage at the blade outlet was lower than that computed at the blade inlet measuring station. Second, the blockage calculated at both the inlet and outlet measuring stations did not vary appreciably with flow.

REFERENCES

1. Lieblein, Seymour; Schwenk, Francis C.; and Broderick, Robert L.: Diffusion Factor for Estimating Losses and Limiting Blade Loadings in Axial - Flow - Compressor Blade Elements. NACA RM E53D01, 1953.

2. Miller, Max J.; and Crouse, James E.: Design and Overall Performance of an Axial-Flow Pump Rotor with a Blade-Tip Diffusion Factor of 0.66. NASA TN D-3024, 1965.

3. Miller, Max J.; and Sandercock, Donald M.: Blade Element Performance of Axial-Flow Pump Rotor with Blade Tip Diffusion Factor of 0.66. NASA TN D-3602, 1966.

4. Crouse, James E.; Montgomery, John C.; and Soltis, Richard F.: Investigation of the Performance of an Axial-Flow-Pump Stage Designed by the Blade-Element Theory - Design and Overall Performance. NASA TN D-591, 1961.

5. Miller, M. J.; Crouse, J. E.; and Sandercock, D. M.: Summary of Experimental Investigation of Three Axial-Flow Pump Rotors Tested in Water. Power, vol. 89, no. 4, Oct. 1967, pp. 589-599.

TABLE I. - VELOCITY DIAGRAM DESIGN VALUES

[Total head-loss coefficient, $\overline{\omega} = 0.125$; $V_{\theta,1} = 0$; $U_{T,1} = U_{T,2} = 99$ ft/sec (30 m/sec).]

Radius ratio, $\frac{r}{r_t}$	Outlet flow coefficient, φ	Relative inlet flow angle, β_1', deg	Change in relative flow angle, $\Delta\beta'$, deg	Rotor head-rise coefficient, ψ	Blade diffusion factor, D
1.000	0.691	55.0	27.8	0.552	0.627
.975	.696	54.3	30.1	.555	.633
.950	.700	53.6	32.5	.558	.637
.925	.704	52.9	35.0	.561	.640
.900	.708	52.1	37.6	.564	.641

TABLE II. - BLADE DESIGN VALUES

[Number of blades, 19; chord length, 1.49 in. (3.78 cm).]

Radius ratio, $\frac{r}{r_t}$	Incidence angle, i, deg	Deviation angle, δ, deg	Camber angle, φ^o, deg	Solidity, σ	Setting angle, v, deg	Ratio of maximum thickness to chord, T_{max}/C
0.99	-8.6	16.9	54.3	1.01	36.2	0.071
.97	-8.5	17.2	56.3	1.03	34.6	.072
.95	-8.5	17.5	58.5	1.05	32.8	.073
.93	-8.5	17.8	60.8	1.08	31.1	.074
.91	-8.4	18.0	63.0	1.10	29.3	.075

TABLE III. - BOUNDARY LAYER BLOCKAGE AT ROTOR INLET AND OUTLET

Ratio of blocked area to total annulus area, percent		
Outer wall, $(A_b/A)_{OW}$	Inner wall, $(A_b/A)_{IW}$	Total, $(A_b/A)_T$
Rotor inlet		
2.29	2.06	4.35
Rotor outlet		
1.46	1.30	2.76

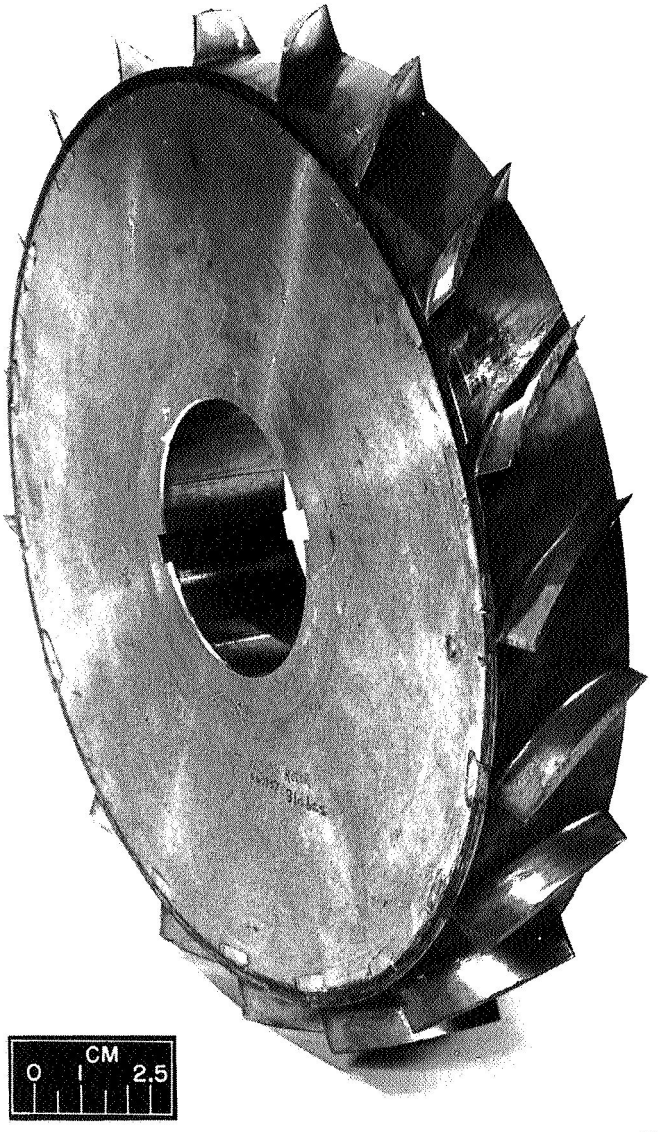

C-69-3580

Figure 1. Rotor.

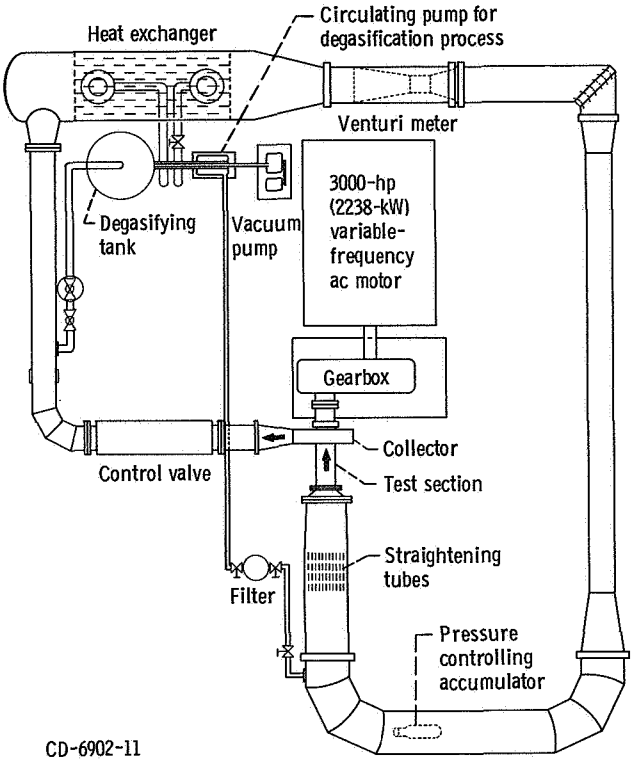

Figure 2. - Lewis water tunnel.

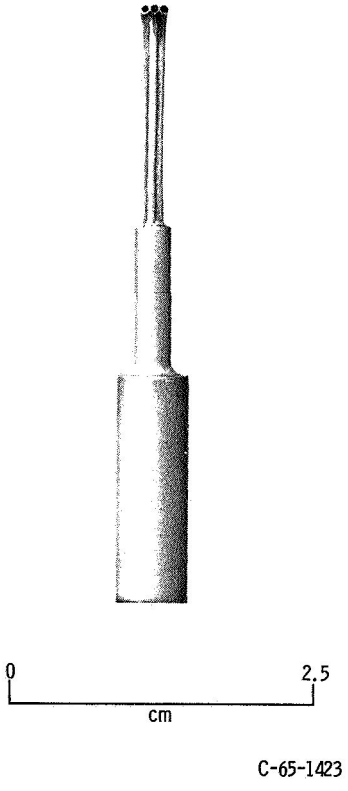

(a) Cobra probe.

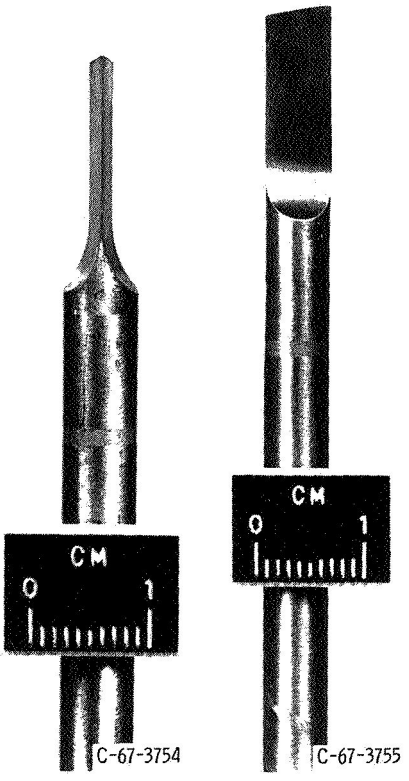

Front view Side view

(b) Static-pressure wedge.

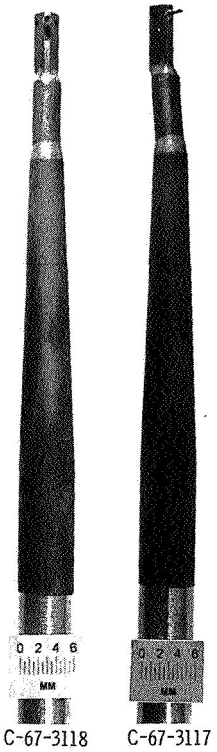

Front view Side view

(c) Boundary-layer probe measuring angle and total pressure.

Figure 3. Probes.

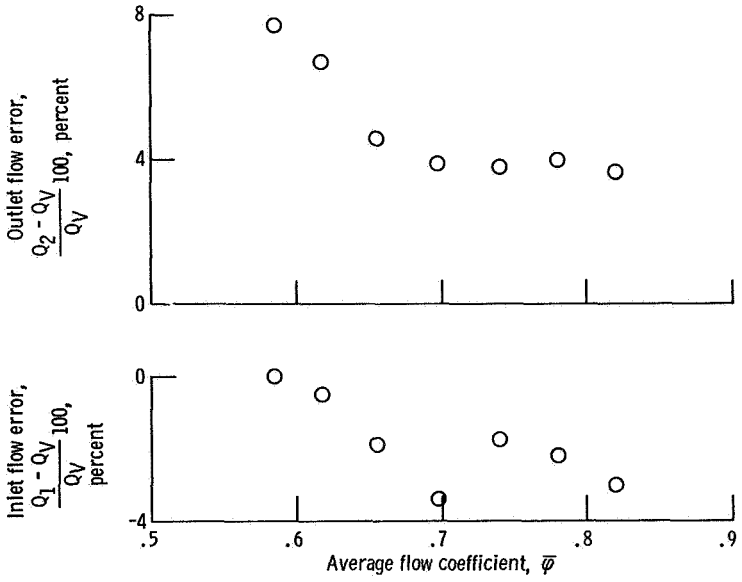

Figure 4. - Comparison of integrated flows at blade inlet and outlet with those measured by venturi meter.

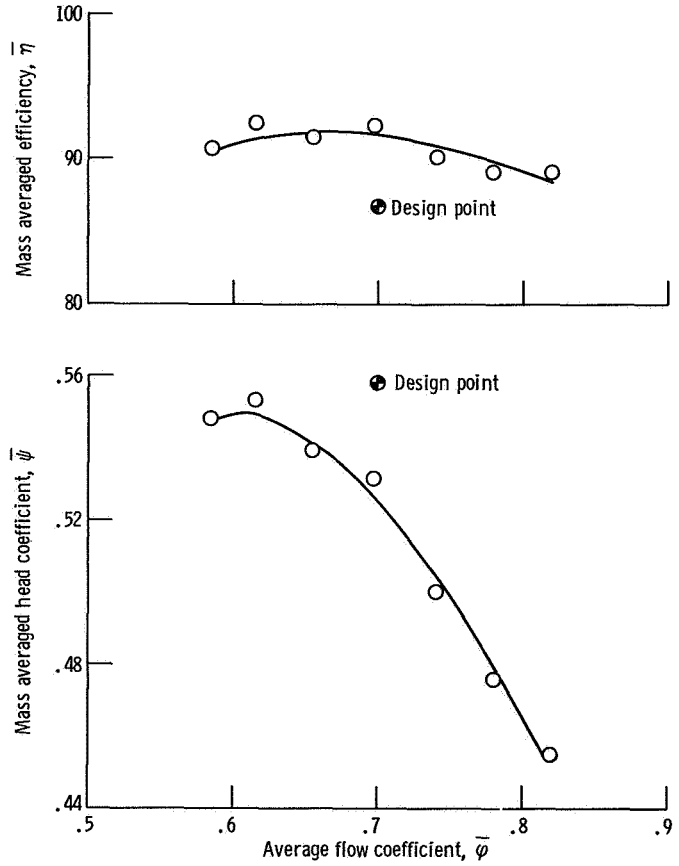

Figure 5. - Overall performance of axial-flow-pump rotor (noncavitating). Rotor-tip speed, 99 feet per second (30 m/sec).

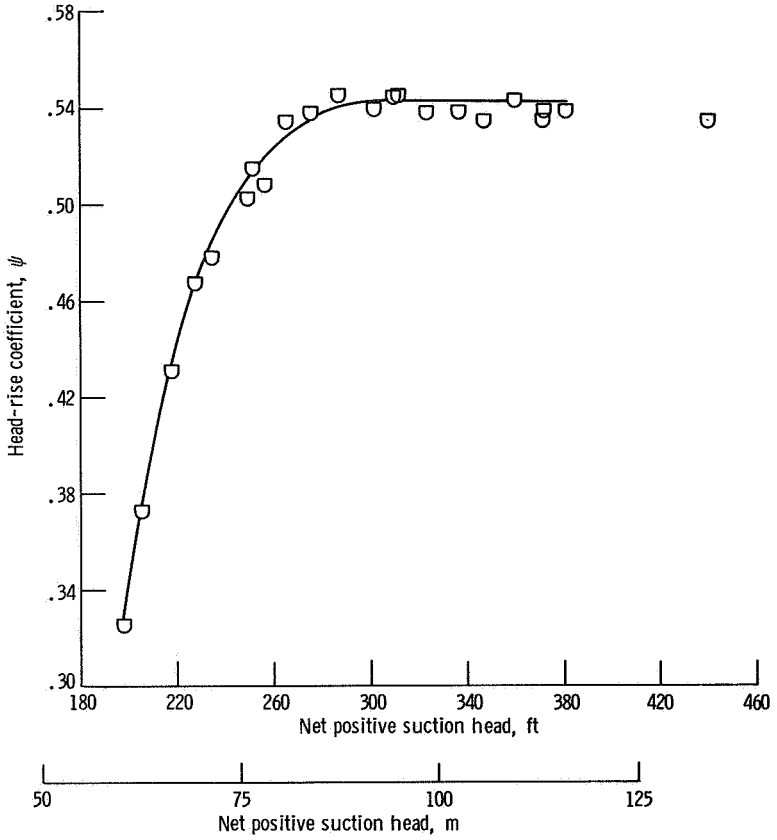

Figure 6. - Effect of cavitation on axial-flow rotor midpoint performance. Rotor-tip speed, 99 feet per second (30 m/sec); average flow coefficient, 0.70.

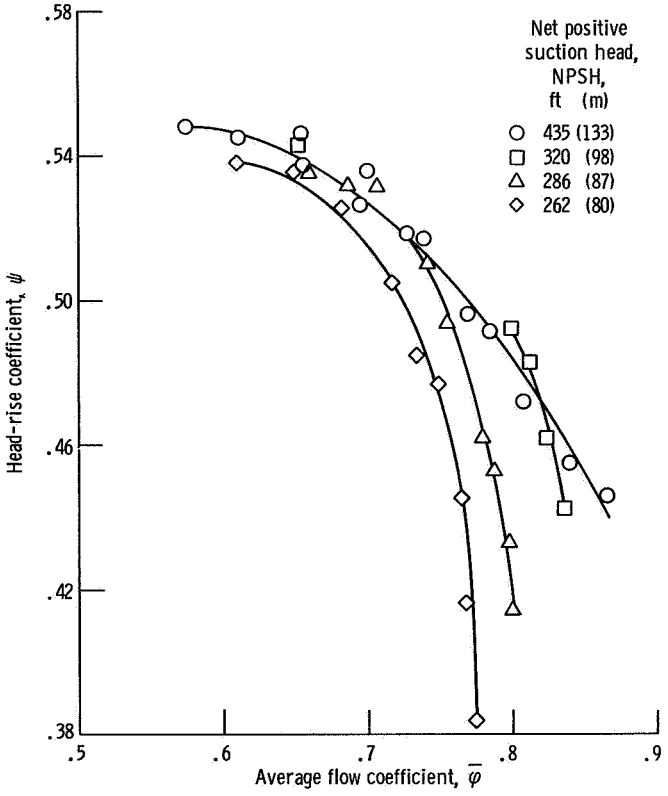

Figure 7. - Midpoint performance curves of axial-flow-pump rotor (cavitating). Rotor-tip speed, 99 feet per second (30 m/sec).

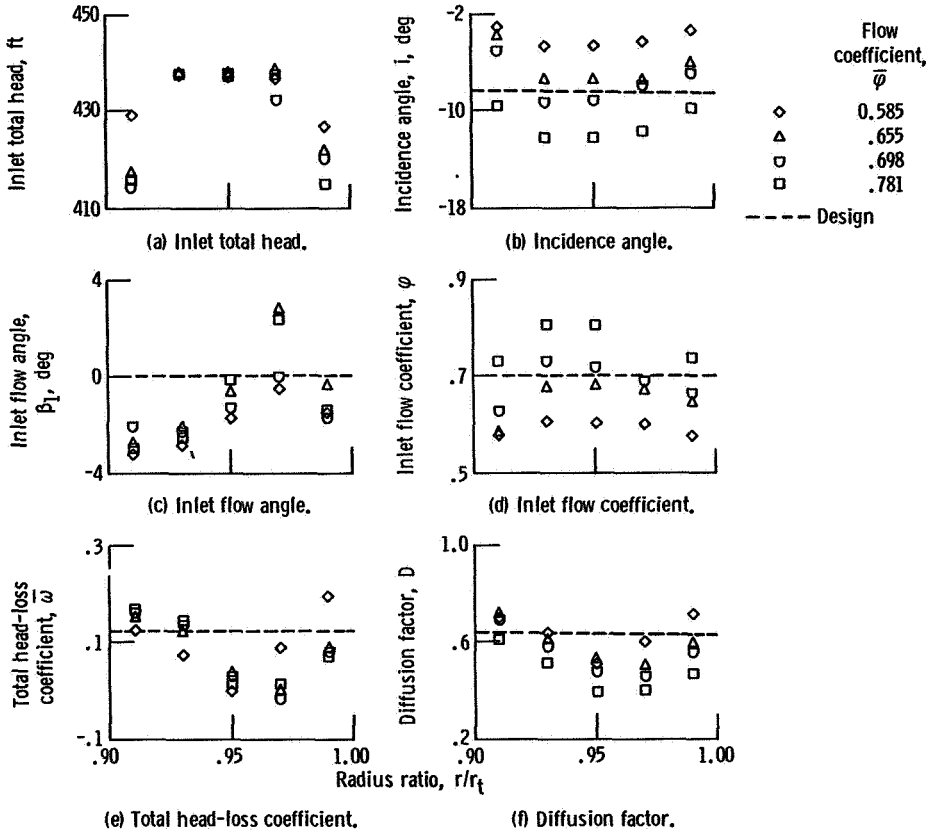

Figure 8. - Radial distributions of blade element flow and performance parameters (noncavitating). Rotor-tip speed, 99 feet per second (30 m/sec); net positive suction head, 428 feet (131 m).

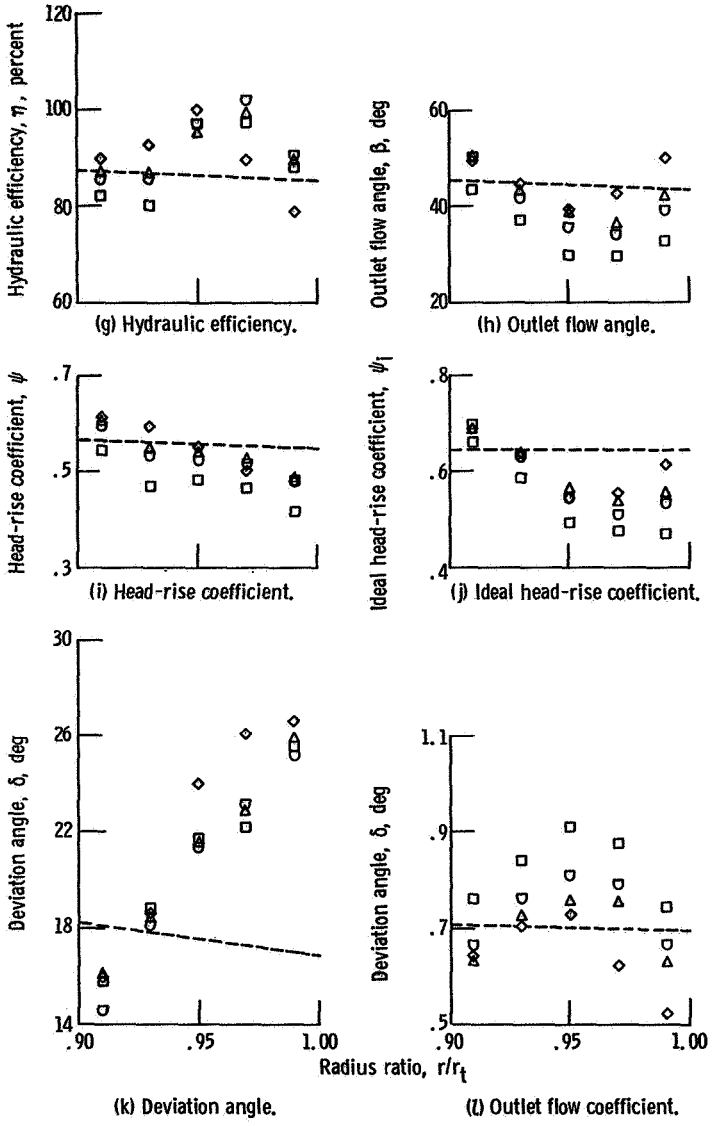

Figure 8. - Concluded.

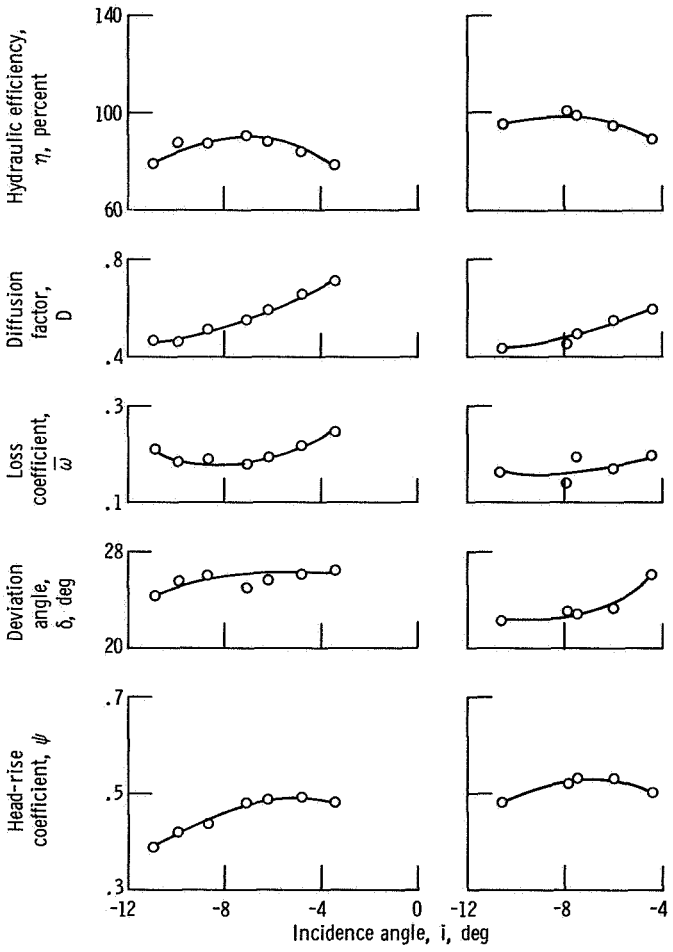

(a) Blade element located at 10 percent of passage height from tip. Radius ratio, 0.99.

(b) Blade element located at 30 percent of passage height from tip. Radius ratio, 0.97.

Figure 9. - Rotor blade element performance characteristics (noncavitating). Rotor-tip speed, 99 feet per second (30 m/sec); net positive suction head, 428 feet (131 m).

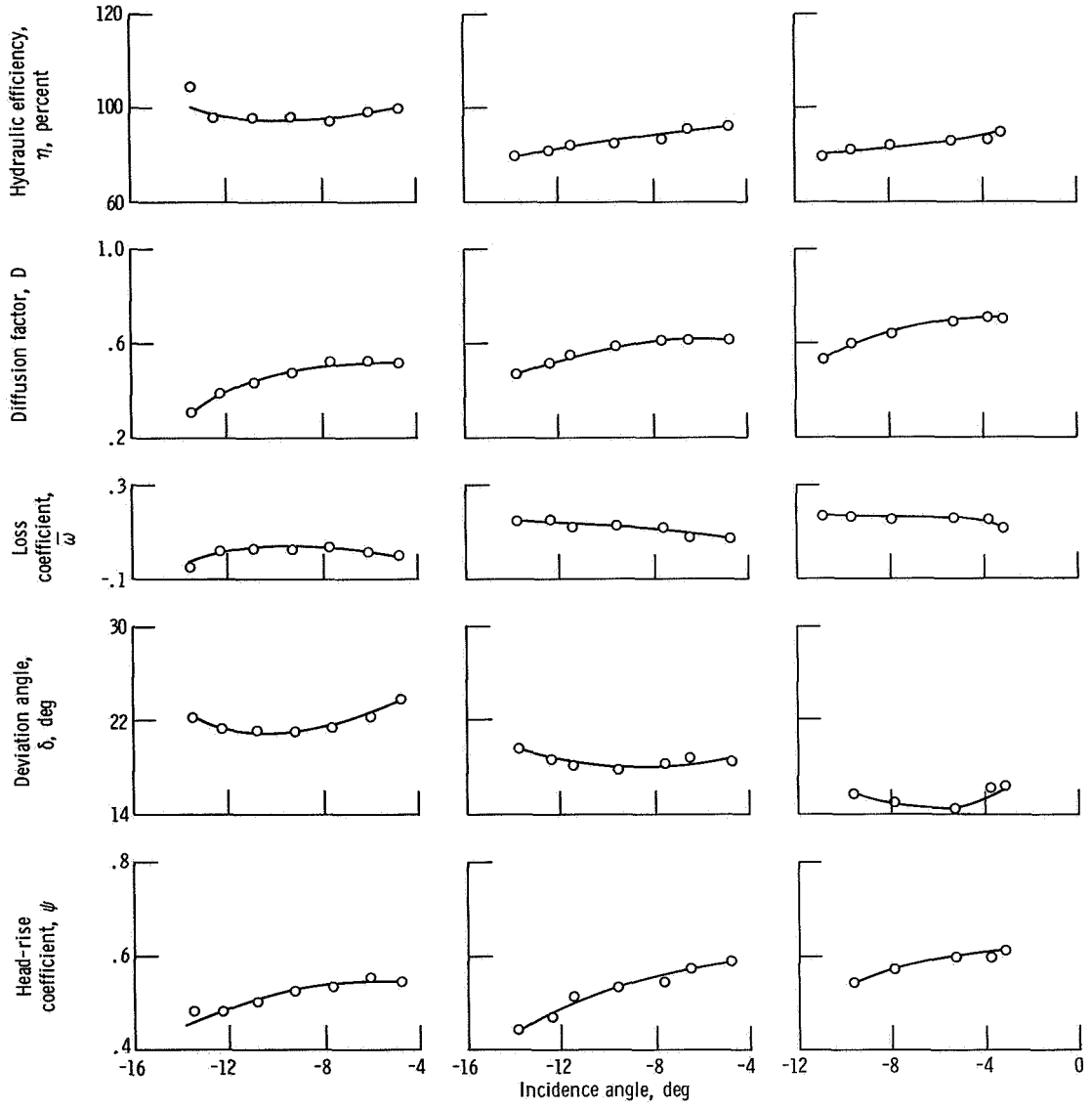

(c) Blade element located at 50 percent of passage height from tip. Radius ratio, 0.95.

(d) Blade element located at 70 percent of passage height from tip. Radius ratio, 0.93.

(e) Blade element located at 90 percent of passage height from tip. Radius ratio, 0.91.

Figure 9. - Concluded.

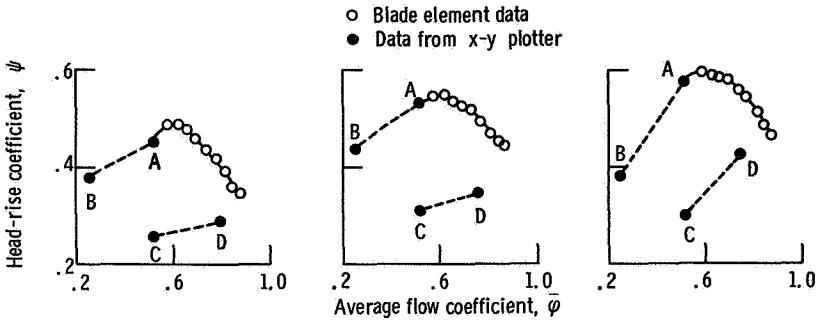

(a) Blade element located at 10 percent of passage height from tip. Radius ratio, 0.99.

(b) Blade element located at 50 percent of passage height from tip. Radius ratio, 0.95.

(c) Blade element located at 90 percent of passage height from tip. Radius ratio, 0.91.

Figure 10. - Rotor blade element performance (noncavitating). Rotor-tip speed, 99 feet per second (30 m/sec); net positive suction head, 430 feet (131 m).

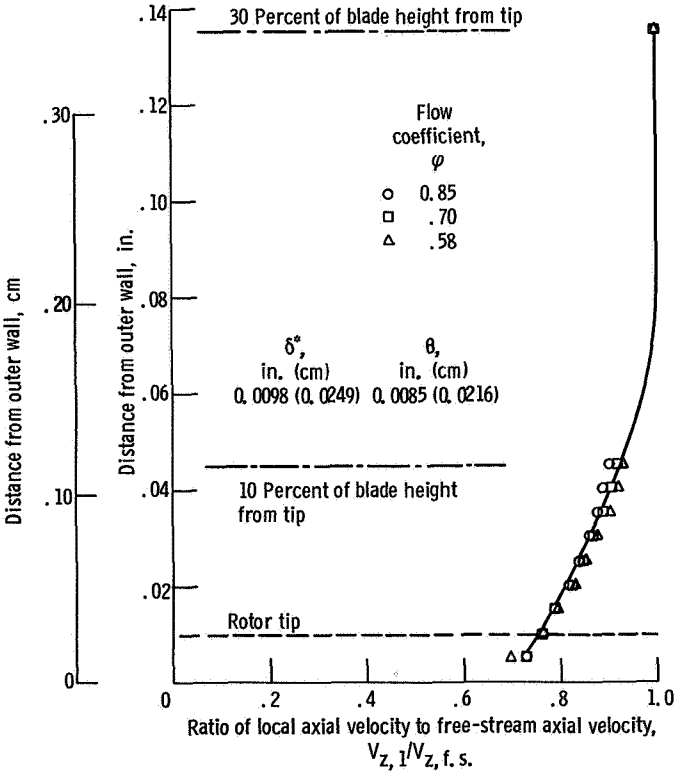

Figure 11. - Velocity distribution across outer wall boundary layer at rotor inlet.

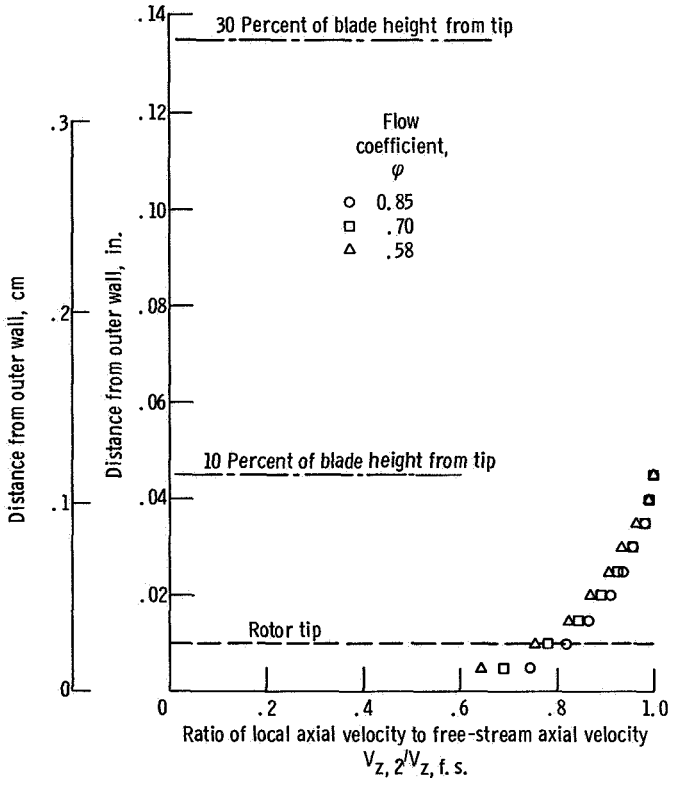

Figure 12. - Axial velocity distribution across outer wall boundary layer at rotor outlet.

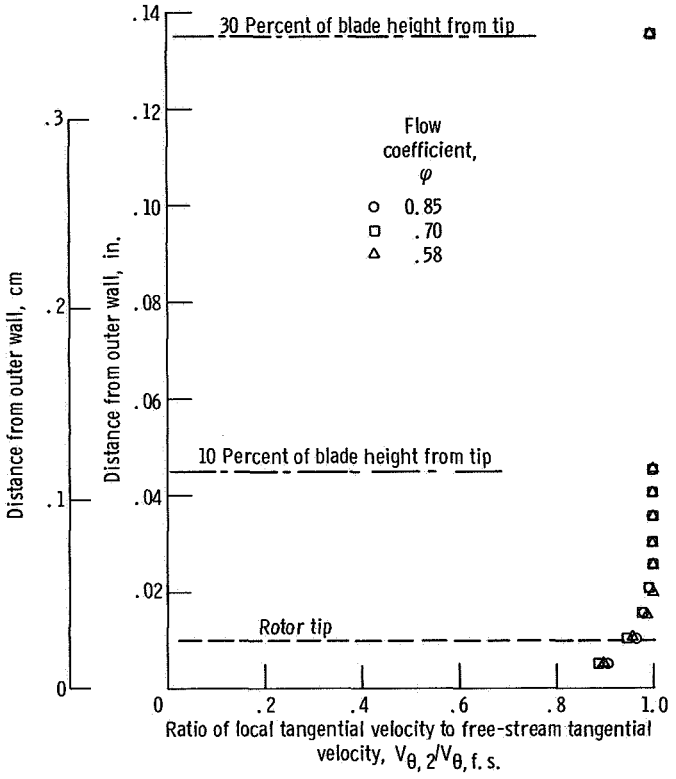

Figure 13. - Tangential velocity distribution across outer wall boundary layer at rotor outlet.

NASA-Langley, 1971 —— 12 E-5765

NATIONAL AERONAUTICS AND SPACE ADMINISTRATION
WASHINGTON, D.C. 20546

OFFICIAL BUSINESS

FIRST CLASS MAIL

POSTAGE AND FEES PAID
NATIONAL AERONAUTICS A
SPACE ADMINISTRATION

POSTMASTER: If Undeliverable (Section 15
Posal Manual) Do Not Retu

"The aeronautical and space activities of the United States shall be conducted so as to contribute . . . to the expansion of human knowledge of phenomena in the atmosphere and space. The Administration shall provide for the widest practicable and appropriate dissemination of information concerning its activities and the results thereof."

— NATIONAL AERONAUTICS AND SPACE ACT OF 1958

NASA SCIENTIFIC AND TECHNICAL PUBLICATIONS

TECHNICAL REPORTS: Scientific and technical information considered important, complete, and a lasting contribution to existing knowledge.

TECHNICAL NOTES: Information less broad in scope but nevertheless of importance as a contribution to existing knowledge.

TECHNICAL MEMORANDUMS: Information receiving limited distribution because of preliminary data, security classification, or other reasons.

CONTRACTOR REPORTS: Scientific and technical information generated under a NASA contract or grant and considered an important contribution to existing knowledge.

TECHNICAL TRANSLATIONS: Information published in a foreign language considered to merit NASA distribution in English.

SPECIAL PUBLICATIONS: Information derived from or of value to NASA activities. Publications include conference proceedings, monographs, data compilations, handbooks, sourcebooks, and special bibliographies.

TECHNOLOGY UTILIZATION PUBLICATIONS: Information on technology used by NASA that may be of particular interest in commercial and other non-aerospace applications. Publications include Tech Briefs, Technology Utilization Reports and Technology Surveys.

Details on the availability of these publications may be obtained from:

SCIENTIFIC AND TECHNICAL INFORMATION OFFICE

NATIONAL AERONAUTICS AND SPACE ADMINISTRATION

Washington, D.C. 20546